




Low-temperature inductively coupled plasma as a method to promote biomineralization on 3D printed poly(lactic acid) scaffolds

John P. Bradford¹, Bernabe Tucker¹, Gerardo Hernandez-Moreno¹, Phillip Charles², and Vinoy Thomas^{1,3,*} 

¹ Polymer and Healthcare Materials/Devices, Department of Material Science & Engineering, University of Alabama At Birmingham, 150 10th Ave South, Birmingham, AL 35294, USA

² Rensselaer Polytechnic Institute, 110 Eighth Street, Troy, NY 12180, USA

³ Center for Nanoscale Materials and Biointegration, College of Arts and Science, University of Alabama At Birmingham, 1300 University Blvd, CH 386, Birmingham, AL 35294, USA

Received: 4 December 2020

Accepted: 1 June 2021

© The Author(s), under exclusive licence to Springer Science+Business Media, LLC, part of Springer Nature 2021

ABSTRACT

For bone tissue engineering, additive manufacturing offers promise in the development of biomimetic scaffolds; however, common polymers used in typical 3D printing methods often suffer from less than ideal surface properties for proper mineralization. As a result, they can underperform with respect to biointegration without additional modification. In this study, low-temperature plasma was utilized to modify the surface of 3D printed poly(lactic acid) (PLA) for promoting mineralization in biomimetic in vitro conditions. Detection of calcium phosphates on the polymer surfaces was accomplished via Fourier transform infrared (FT-IR) spectroscopy and X-ray photoelectron (XPS) spectroscopy. Scanning electron microscopy (SEM) was employed to identify and image the mineralization products on the surfaces of the scaffolds. Further, a fluorescent assay of surface extracts identified calcium-containing mineral deposits at significantly higher levels for treated scaffolds versus controls. Taken together, these results suggest the futuristic potential of this surface modification method for bone tissue engineering applications.

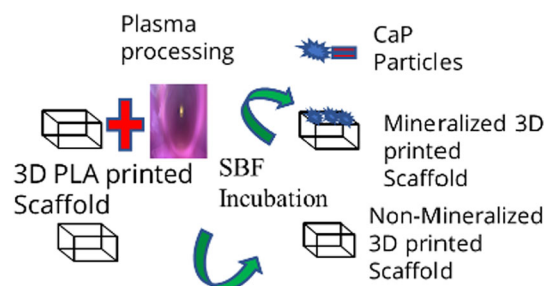
Handling Editor: Annela M. Seddon

Address correspondence to E-mail: vthomas@uab.edu

<https://doi.org/10.1007/s10853-021-06227-z>

Published online: 14 June 2021

GRAPHICAL ABSTRACT



Introduction

Bone tissue engineering has faced many innovations in recent years. Being able to produce implants that mimic the native mechanical and biological properties of human bone would be incalculably beneficial [1]. Synthetic polymeric scaffolds are among the top choices to fill this role due to their bioactivity, biocompatibility, tunable degradation, and varying forms [2–4]. The rationale behind using polymers for bone tissue engineering scaffolds, despite inferior mechanical properties, is their weakening of mechanical properties as they degrade with time. This allows for bone tissue to gradually be introduced to load of standard bodily conditions which aids in the natural healing process [5]. For polymeric scaffolds to be utilized, to replace other material classifications, they must have a higher level of biocompatibility, bio-integration, and bioactivity while possessing mechanical properties sufficient for biological function [6, 7]. Poly(lactic acid) (PLA) is one such polymer, derived from natural and renewable resources, degrades *in vivo* conditions to lactic acid which follows normal human metabolism, and finally degrades to amiable products [8–10]. Facile processing of PLA allows it to be used in a variety of applications such as food packaging [11], as absorbable sutures [12], textile use [13], and drug delivery [14–16].

Recent advances with technology have led to the incorporation of techniques such as 3D printing and low-temperature plasma (LTP) modification in the search for suitable biocompatible materials

processing [17]. 3D printed scaffolds are advantageous in that they, upon implantation, help to regenerate damaged tissue and allow flexibility in degree of porosity which helps vary the biomedical applications in which it can be employed [5, 18, 19]. Calcium phosphate (CaP) is a precursor to inorganic hydroxyapatite (HAP) which makes up a large portion of the composition of bone tissue [20]. From the previous literature, CaP, in the form of several phases, is biomineralized, directly synthesized, or used as a composite to benefit bone tissue engineering. Ivanova used various plasma treatments to biomineralize calcium carbonate on a electrospun scaffold [21]. Xudong synthesized PLA microspheres and utilized oxygen plasma in biomimetic conditions which caused increased amount of HAP to biomineralize on the microspheres [22]. Li made chitosan scaffolds and impressively caused mass mineralization on the scaffold by inducing porosity on the scaffold using a basic solution and a chemical degradation to smaller chemical fragments using a ethanol-water solution in only 2 days [23]. This method, however, used a strongly basic solution to induce porosity which would detriment the mechanical properties and cause degradation to many polymers utilized in bone tissue engineering [24–26], and since mineralization was not in biomimetic conditions, *i.e.*, in simulated body fluid (SBF) or synonymous conditions, the morphology of the crystal structure of the HAP biomineralized will likely differ from that which is naturally formed in biomimetic conditions, thus possibly affecting cell proliferation on the scaffold [24, 27]. To the authors knowledge, a gap in literature exists as to whether a

facile and more mild method of surface treating a 3D printed PLA scaffold, by using LTP, for the mineralization of a CaP mineral, alone can significantly effect mineralization efficiency. LTP utilization for increasing bioactivity can prove advantageous in that the method is simple to vary the surface chemistry of the scaffold while LTP does not effect the bulk properties of the material [21, 28, 29]. This will produce a mineralized surface covering that will form in the morphology synonymous to that in the body, without compromising the integrity of the scaffold.

In this study, PLA 3D printed scaffolds were surface treated using LTP to determine whether this benign surface treatment on a 3D printed scaffold could significantly increase the amount of CaP deposited on the surface in biomimetic conditions.

Experimental

Materials

Commercial-grade poly(lactic acid) filament (PLA; US Plastics Corp.TM, natural, 3 mm diameter) was utilized for the 3D printed scaffolds. Sodium hydroxide pellets, extra pure sodium chloride, 99% pure anhydrous sodium sulfate, potassium phosphate dibasic trihydrate, and sodium bicarbonate came from Arcos Organics. Anhydrous calcium chloride and tris hydroxymethyl aminomethane ultrapure(Tris) came from Alfa Aesar, and magnesium chloride hexahydrate came from Fischer Scientific, and ultrapure potassium chloride and calcein came from Sigma-Aldrich.

Scaffold preparation

PLA scaffolds dimension ($3.105 \times 1.14 \times 0.518$) cm were 3D printed on a LulzBot mini using cura as the programming software, and the bulk density of the scaffolds is 0.421 ± 0.0803 and 0.443 ± 0.0328 for $n = 3$ where the p-value for the student *t*-test is 0.45 for these two groups. The filament was extruded at 195 °C through a 0.5-mm nozzle. After extrusion onto the bed of the 3D printer, the scaffolds were then slowly removed and immediately experimentally utilized.

Scaffolds were placed into a plasma cleaner (Harrick PDC-001) and were plasma treated at 0.200 torr for 30 min on each side of the scaffold using

ethylenediamine (EDA) plasma. The plasma-treated and control scaffolds were immediately placed in a 10-mL glass jar and submerged in $1.5 \times$ SBF for 18 days made as described by XuDong briefly [22]:

For a preparation of a 500 mL solution of SBF, the following was added to 500 mL of deionized (DI) water and stirred vigorously: 5.997 g of NaCl, 0.263 g NaHCO₃, 0.168 g of KCL, 0.172 g of K₂HPO₄ 3H₂O, 0.0229 g MgCl₂ 6H₂O, 30 mL of 1 M solution of HCl, 0.208 g of CaCl₂, 0.0503 g of Na₂SO₄, and 4.543 g of Tris. The solution was buffered to a pH of 7.40 ± 0.02 using the HCl solution.

The scaffolds in the SBF solution were incubated at $37 \text{ }^\circ\text{C} \pm 1 \text{ }^\circ\text{C}$. The SBF solution was changed every 72 h to refresh the ion concentration. After 18 days, the scaffolds were removed from the solution, and gently washed with deionized water and dried under vacuum for 96 h before conducting characterization.

Characterization of scaffold

Water contact angle (WCA) for wettability

Wettability of the neat PLA scaffold was resolved by static water contact angle. A water droplet was placed onto the EDA treated and control neat PLA scaffolds at room temperature by a Chemyx syringe infusion pump, set a rate of 50 μL per minute, until a water droplet was fully formed on the surface. The images were captured by a Wild Heerbrugg M5-64,666, and the evaluation was performed by ImageJ software. Seven measurements were made for each of the groups, and the average value was reported with the standard deviation.

Scanning electron microscopy (SEM) for morphology

SEM images were acquired with a Quanta FEG 650 Scanning Electron Microscope under high vacuum in order to identify structure and morphology of the processed 3D printed scaffolds, in addition to qualitatively measure the difference of biomineralized material on the surface of the scaffolds. To reduce charging on the surface of the scaffold, the samples were sputtered using an Au-Pd coating which increase surface conductivity. The parameters ran at 10 kV with varying spot sizes.

X-ray photoelectron spectroscopy (XPS) for surface chemistry

XPS was performed using PHI 5000 Versaprobe imaging XPS. The X-ray source of this instrument is a monochromatic, focused, Al K-alpha source ($E = 1486.6$ eV) at 25 W with a 100 μm spot size. An argon ion gun was used to prevent any charging in the spectra by neutralizing the charge. The software utilized for analysis of the spectra is the Multipak v9.0 software.

Fourier transform infrared spectroscopy (FTIR) for surface chemistry

FTIR was performed with a Bruker alpha system, via ATR mode, to identify chemical functional groups on the surface of the scaffolds. The infrared spectrum was recorded in the range of $(4000\text{--}400)$ cm^{-1} at 64 scans/min.

Calcein staining (for biomineralization)

The scaffolds (both treated and control) were sonicated in deionized water for 5 min and dried. They were then sonicated in a 1 M NaOH solution. 99 μL of the NaOH solution was taken and placed in a well plate in addition to 1 μL of a 0.02 M calcein solution and analyzed under UV light for fluorescence. The excitation source was a 20-W halogen bulb feeding a fiber optic cable through a narrow filter (490 nm center, 10 nm bandpass) at 45° to the sample. The CMOS detector (5.0 megapixel with $f/4$ 50 mm lens) captured the emitted fluorescence through another narrow filter (530 nm center, 10 nm bandpass) at normal angle to the sample. ImageJ was used to quantify the pixel intensity of fluorescence signals using a macro-plugin custom written to extract pixel values from raw RGB images. No additional processing was used for pixel quantitation. Cyan hot LUT was employed for the image enhancement of the comparative samples to use in a qualitative comparison to better visualize in the figure.

Mechanical characterization of scaffolds

The mechanical properties of the 3D printed PLA scaffolds were measured using TA instruments RSA-G2 dynamic mechanical analyzer in 3-point bending mode. The scaffolds were compressed with a sphere

head normal to the scaffold and oscillated with fixed forces (40, 200, 500 $\text{g}\cdot\text{force}$), and the storage modulus of each was determined by varying the frequency from 0.1 to 100 Hz at a fixed strain of 0.05% in ambient conditions.

Results and discussion

When comparing SEM images from Fig. 1a and c, the control and treated samples, respectively, there is a quantitatively higher ratio of biomineralized product (the white particles displayed in the images) in the treated sample than the control sample. When running higher magnification as shown in 1b and 1d, the control and treated sample, respectively, there is a substantial amount of biomineralization, nearly covering the entire surface as compared to the control sample in Fig. 1b. The IR peaks for both carbonate (CO_3^{2-}) and phosphate (PO_4^{3-}) were gathered from prior information [24, 30, 31]. PLA has characteristic peaks that overlay with both CO_3^{2-} and PO_4^{3-} groups as shown in Fig. 2. The intensity of the peaks was analyzed, in order to demonstrate the sample with higher quantity of both CO_3^{2-} and PO_4^{3-} . The peaks associated with both the CO_3^{2-} and PO_4^{3-} had a higher intensity in the treated samples than both the control and neat samples [24, 30, 31]. This is attributed to the heightened biomineralization that occurred as a result of EDA based LTP.

The XPS results further support this because of the significant difference in the quantity of CaP that is biomineralized on the surface of the treated sample versus the untreated sample, where Fig. 3 displays the XPS spectra before and after the biomineralization process. Table 1 shows the effectiveness of the EDA plasma treatment by significantly increasing the wettability of the 3D printed scaffold as shown by the decrease in the water contact angle of the EDA-treated scaffold versus the control scaffold. Table 2 shows that there is approximately more than 3 times more CaP on the EDA surface-treated sample versus the control.

One theory why this surface treatment affects the biomineralization is LTP treatment creates small pockets in the 3D printed scaffolds that become both thermodynamically and kinetically more favorable for the nucleation of CaP [23, 32]. Another theory is that increased amine functionalization on the surface that is created due to using EDA plasma causes

Figure 1 **a** Low and **b** high magnification of the control biomineralized scaffold, **c** is the low and **D** high magnification of the plasma-treated scaffolds. All scaffolds were immersed in SBF for 18 days.

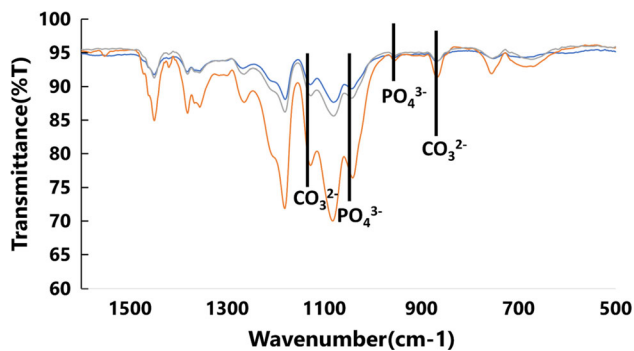
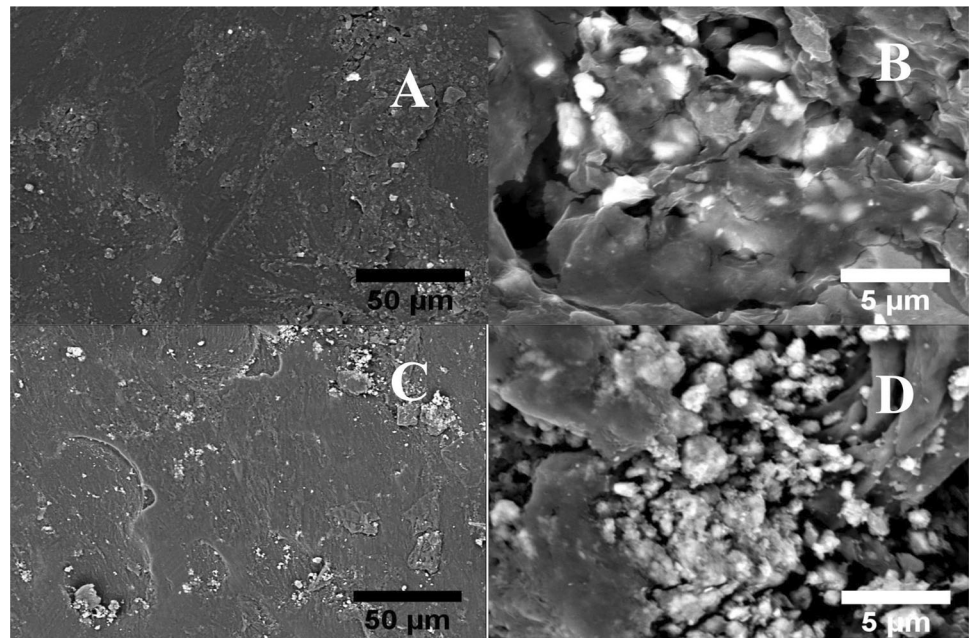


Figure 2 FTIR results of biomineralization study at day 18. The peak positions of the CO_3^{2-} and the PO_4^{3-} groups are outlined as displayed. The spectrum in orange show the PLA scaffold that was treated and immersed in SBF for 18 days, the spectra in gray show just the 3D printed PLA scaffold, and the blue displays the PLA scaffold that was not surface treated, but immersed in SBF for 18 days.

additional chelation of the calcium ions that are present in the SBF, followed by the binding of phosphate ions by the calcium [23, 32–37]. Both theories influenced the methodology used where the treated 3D printed scaffolds were intentionally etched with EDA plasma, by treating each side of the 3D printed scaffold with EDA plasma for 30 min. This created pores, most probable nanosize based on the size of the CaP mineralized, within the scaffolds that caused CaP to nucleate within those pores. Tables 1 and 2 show the elemental composition of the

scaffolds where the atomic percentage of carbon and oxygen makes up the majority of each scaffold.

Ca^{2+} ions binds to free amines on the surface of the treated scaffold that was induced by LTP using EDA [21, 34]. This explains the higher atomic percent of nitrogen on the control scaffold, which indicates little mineralization of CaP, versus the treated scaffold.

The chemical composition of PLA is known to be elementally composed of carbon and oxygen, so any other atomic composition displayed in XPS is from the biomineralization processing, plasma processing, or exposure to the environment between characterization and processing. The small quantity of nitrogen appearing on the treated scaffold after biomineralization implies maximum chelation on the surface of the scaffold, which shows that 18 days at $1.5 \times$ SBF is an optimum and efficient period of time for biomimetic treatment of PLA scaffolds, as shown in Table 2. Figure 4 shows a higher magnification of the mineralized product on the surface of both the treated and control samples which gives visual detail to the morphology.

This morphology difference observed in Fig. 4 between the treated and control sample gave the implication that CaP complexation did not occur in the control sample. CaP, in all different phases, has specified morphology that like in Fig. 4a and b is clearly observed [20, 33]. The deposition on the control sample is most likely salt from the SBF solution,

Figure 3 **a** XPS spectra of a the 3D printed PLA sample. **b** XPS spectra of the 3D printed PLA sample that was plasma treated with EDA. **c** XPS spectra of the EDA plasma-treated sample that was immersed in SBF for 18 days. **d** XPS spectra of the control sample that was immersed in SBF for 18 days.

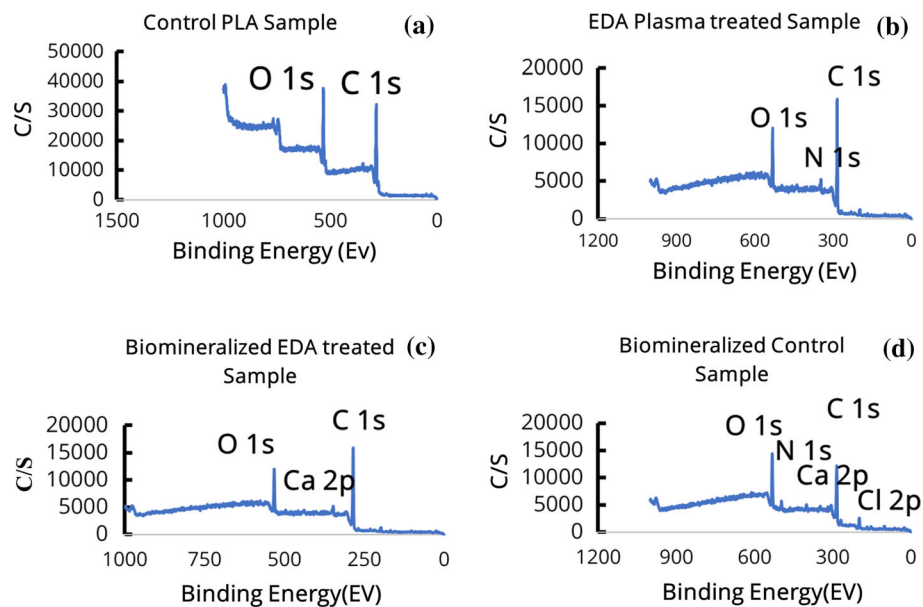


Table 1 Surface elemental analysis before biomineralization

	Neat EDA treated	Neat Control
Water contact angle(°) <i>n</i> = 7	18.32 ± 0.17	67.57 ± 0.85
XPS Carbon (at %)	63.9	74
XPS Oxygen (at %)	29.6	26
XPS Nitrogen (at %)	6.5	N/A
XPS N:C ratio	6.5:63.9	N/A

Table 2 XPS analysis after biomineralization

Element	Control atomic (%)	Treated atomic (%)
C	64.8	78.9
O	24.8	18.2
N	3.5	< 0.1
Cl	3.3	1.2
Si	2.7	N/A
Ca	0.5	1.7
S	0.5	N/A

whereas the mineralized surface of the treated sample appears to have agglomerated mineralized CaP.

Calcein complexes with several different metals. Differentiation between complexing with free Ca²⁺ and CaP is essential for a quantitative measurement of CaP biomineralized on the scaffold. Extensive washing of each scaffold with water, through

sonication, removed any free salts on the surface of the scaffold which allows for the calcein staining to be performed free of any Ca²⁺ ions, outside of a small amount of auto fluorescence due to the calcein solution, while CaP minerals would remain in the scaffold, which is indicative of the effectiveness of EDA plasma treatment in creating nucleation sites for biomineralization. While previous research indicates that processes such as aminolysis are effective [38–40], LTP is a known alternative to make these nucleation sites without compromising the mechanical properties or causing degradation of the polymer [41]. Sonication of the water washed product in strong basic solution afterwards allowed for any CaP mineralized on the scaffold to be dissolved in the solution, which was then treated with calcein. This means the fluorescence due to the staining would be of the mineralized product only, as no free Ca²⁺ ions were on either scaffold as shown in Fig. 4. Knowing that calcein binds to other metals, using NaOH as the basic solution not only dissolved the biomineralized product, but made the pH 13.3 ± 0.1. In the pH range of 13–13.5, calcein binding becomes selective to calcium-containing complexes; thus, any fluorescence seen in Fig. 4 is attributed only to the CaP biomineralized product [42]. SEM images were used to further quantify the difference in particles between control and treated scaffolds. Figure 5 demonstrates a difference in product mineralized on surface by using a difference in contrast between mineralized product

Figure 4 High-magnification images focused on mineralized product. **a** and **b** (LTP treated) were taken at 30 K and 60 K, respectively, and display crystallite morphology. **c** and **d** (untreated controls) were taken at 2 K and 10 K magnification, respectively, where the morphology is salt-like.

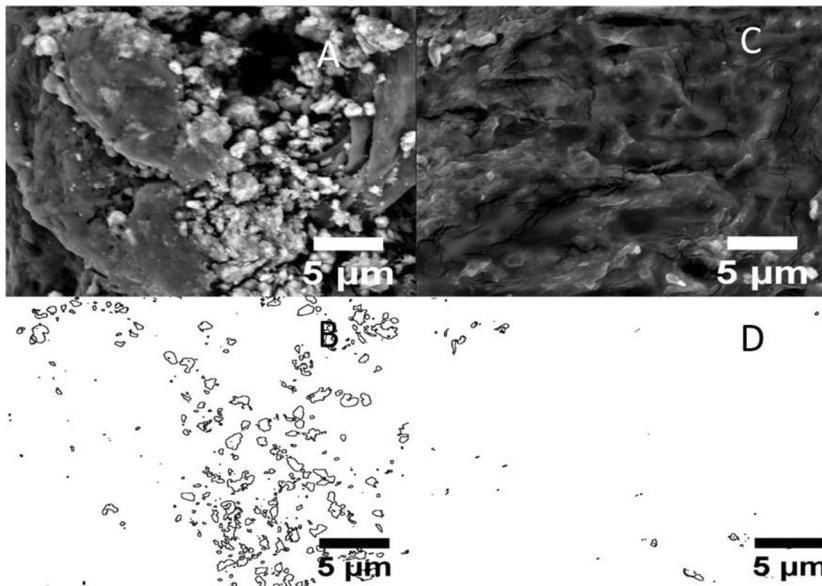
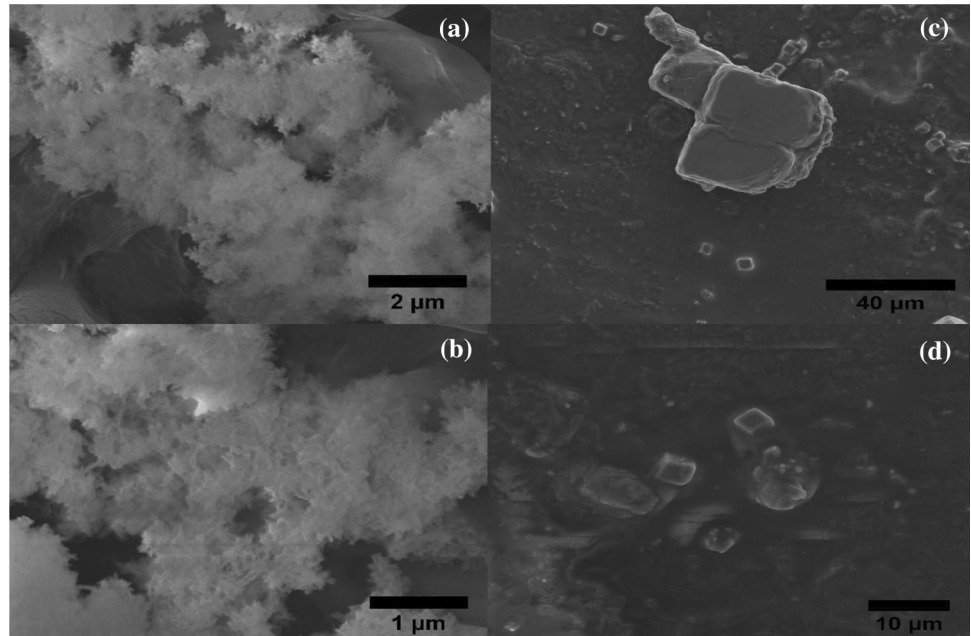
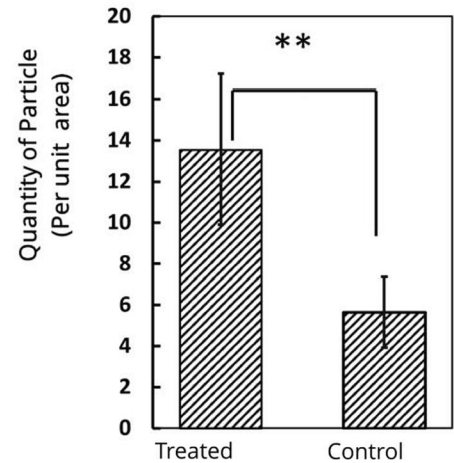


Figure 5 Representative SEM images of treated samples (**a**, **b**) and control samples (**c**, **d**). Raw unaltered grayscale images (**a**, **c**) were used for quantification. Processed images (**b**, **d**) are shown to demonstrate the difference; with ImageJ, the processed images were threshold to eliminate the background, inverted LUT, and

and matrix in ImageJ and performing an area count of remaining particles.

To statistically determine the difference in fluorescence, between the control and treated samples, a Student *t*-test was ran on the calculated pixels from each image displayed in the graph in Fig. 6.



edges found for particle quantification. The particle count per unit area is 13.54 ± 3.66 and 5.65 ± 1.72 for the treated and control samples, respectively, with an $n = 7$ for each sample. Error bars are in accordance with the standard deviation with each group. The computed *p* values were < 0.001 .

The Student *t*-test determined that the amount of fluorescence from the treated to control sample is statistically different where the (p -value < 0.05) which communicates that these values are substantially different where the low standard deviation for both samples indicates repeatability of the study. With the small amount of calcein utilized in the

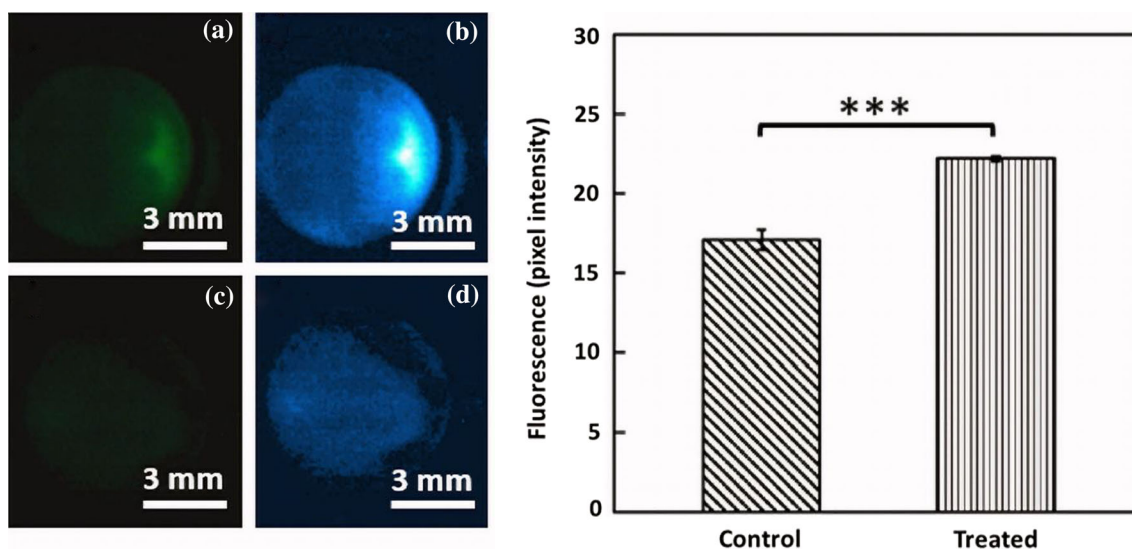


Figure 6 Representative fluorescent assay images of treated samples (a, b) and control samples (c, d). Raw unaltered RGB images (a, c) were used for quantification. Processed images (b, d) are shown to demonstrate the intensity difference; with ImageJ, the green channel was contrast enhanced and the cyan hot LUT added for clarity. Bars are 3.0 mm. Graphical results of the fluorescence

sample, reference the experimental section, the calcein gathered in one section of the well plate, so when pixel values were collected to calculate fluorescence values for both control and treated samples the section in which the calcein gathered was specifically measured to help minimize variability in the results. Figure 6 shows both the fluorescent samples along with the amount of pixels that each sample contains as a result of the amount of CaP each sample contained. ImageJ was used in order to calculate the fluorescence of both control and treated samples, and in order to eliminate biases in the calculation a plug in program was utilized for each of the measurement which measured the same area of each sample. Plasma-processed EDA on the surface of 3D printed PLA facilitated calcification through chelation as reported elsewhere [43]. The calcium ions form a complex with electronegative nitrogen (donor atom) of plasma-polymerized EDA chains present within the coordination sphere. Once calcium ions bind through chelation, they will attract phosphate anions and propagate more CaP mineralization. Recently, we have reported an overview of LTP plasma effect on the surface structuring and mineralization of bioimplants [44].

The mechanical and bulk density properties between the control and treated groups showed a

quantity are 22.21 ± 0.17 and 17.09 ± 0.62 for the treated and control samples, respectively, average of $n = 15$ for each with error bars for the standard deviation. The computed P value found to be < 0.001 and was performed in Microsoft Excel by a Student t -test.

small difference, but statistically insignificant difference between the two groups. Figure 7 displays the mechanical properties as it pertains to different forces applied to the scaffold and between the control and treated groups.

The mechanical and porosity data both showed slightly higher attributes in favor of the treated group in comparison to the control, but neither is statistically significant. As displayed in both Figs. 1 and 4, the size of the CaP particles is nanometer scale, when compared to the bulk size of the scaffolds, centimeter in scale. This displays why the difference in the bulk density (directly related to the porosity) is not statistically significant. As denoted in prior studies [45], difference between the two groups while also demonstrating an increase biomineralization on this group of scaffolds (plasma treated and non-treated) is not sufficient for increasing the mechanical properties. The resulting P value (from the student t test) on the bulk density between the treated and control groups was 0.45 (Fig. 7) when either different forces applied to each scaffold or the two processed groups are compared. Therefore, the quantitative variation between the groups is not high enough to denote a relationship in between mechanical properties and biomineralization of CaP on 3D printed PLA scaffolds.

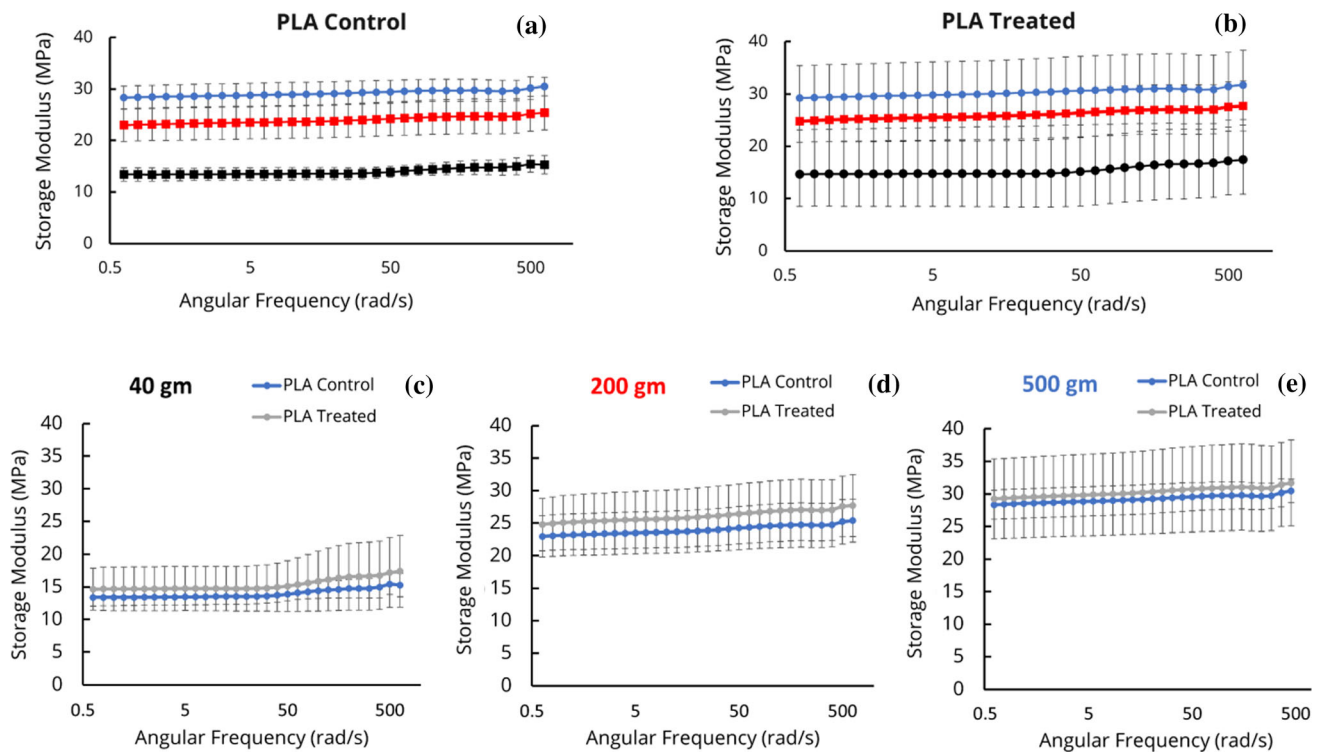


Figure 7 Mechanical data displaying the how the storage modulus varies with angular frequency. Three different forces were applied (40, 200, and 500 g force) across the frequency spectrum to show the behavior of each group with varying force. (a, b) display the mechanical behavior of the 3 forces on each

biomineralized group, where the resulting storage modulus decreased with decreasing force applied (blue is 500 gm, red is 200 gm, and black is 40 gm). (c, d and e) show the same data but where the samples are compared to each other relative to the force applied. The error bars on all signify the standard deviation.

Conclusion

LTP was successfully shown to be a viable agent in inducing biomineralization of CaP in 3D printed scaffolds for the improvement in the mineralization of 3D printed polymer scaffolds. LTP allows for induction of additional nucleation sites and functionalization of the surface to promote chelation of the Ca^{2+} ions, allowed significantly greater formation of the CaP mineral on the surface of the 3D printed scaffold. Special care was taken to differentiate between mineral formation and free ion residue from the biomimetic treatment. Biomimetic conditions were utilized in an attempt to tailor the morphology of the mineralized product to closely mimic that which is naturally formed in the body. To the writers' knowledge, this is the first time for LTP being used to create the nucleation sites on PLA 3D printed scaffolds to induce CaP growth on the scaffold. Morphological difference between mineralized products happened as a result of using atmospheric plasma. Further studies will need to include biological studies

to confirm biocompatibility of CaP mineralized product, with this specific morphology, in regard to bone cells.

Acknowledgements

The authors acknowledge support by the Department of Education GAANN Grant No. P200A180001, as well as National Aeronautics and Space Administration (NASA)-Alabama Space Grant Consortium, Research Experiences for Undergraduates (REU) award to UAB NSF EPSCoR CPU2AL: Connecting the Plasma Universe to Plasma Technology in Alabama, funded through Cooperative Agreement OIA-1655280. We would also like to thank Dr. Paul Baker for his assistance in characterization with XPS, and the SEM instruments and Mr. Pravin Dimple for help in 3D printing. The funders had no role in the design of the study; in the collection, analyses, or interpretation of data; in the writing of the manuscript; or in the decision to publish the results.

Author contributions

VT, JB, and PC took part in conceptualization. VT, JB, GHM, PC, and BT involved in methodology. JB, BT, and IS took part in formal analysis. JB and GHM involved in investigation. VT took part in resources. JB, PC, and GHM participated in data curation. JB and BT involved in writing—original draft preparation. VT took part in writing—review and editing, visualization, supervision, project administration, funding acquisition. All authors have read and agreed to the published version of the manuscript.

Declarations

Conflict of interest The authors declare that they have no conflicts of interest.

References

- Grémare A, Guduric V, Bareille R et al (2018) Characterization of printed PLA scaffolds for bone tissue engineering. *J Biomed Mater Res, Part A* 106:887. <https://doi.org/10.1002/jbm.a.36289>
- Teo AJT, Mishra A, Park I, Kim Y-J, Park W-T, Yoon Y-J (2016) Polymeric biomaterials for medical implants and devices. *ACS Biomater Sci Eng* 2:454. <https://doi.org/10.1021/acsbomaterials.5b00429>
- Kariduraganavar MY, Kittur AA, Kamble RR (2014) Natural and synthetic biomedical polymers. Elsevier, Oxford
- Zhu L, Luo D, Liu Y (2020) Effect of the nano/microscale structure of biomaterial scaffolds on bone regeneration. *Int J Oral Sci* 12:6. <https://doi.org/10.1038/s41368-020-0073-y>
- Maurus PB, Kaeding CC (2004) Bioabsorbable implant material review. *Operat Techn Sport Med* 12:158. <https://doi.org/10.1053/j.otsm.2004.07.015>
- Wood AT, Everett D, Kumar S, Mishra MK, Thomas V (2019) Fiber length and concentration: synergistic effect on mechanical and cellular response in wet-laid poly(lactic acid) fibrous scaffolds. *J Biomed Mater Res Part B, Appl Biomater*. <https://doi.org/10.1002/jbm.b.34125>
- Song R, Murphy M, Li C, Ting K, Soo C, Zheng Z (2018) Current development of biodegradable polymeric materials for biomedical applications. *Drug Des Devel Ther* 12:3117. <https://doi.org/10.2147/DDDT.S165440>
- Wood AT, Everett D, Budhwani KI, Dickinson B, Thomas V (2016) Wet-laid soy fiber reinforced hydrogel scaffold: fabrication, mechano-morphological and cell studies. *Mater Sci Eng, C* 63:308. <https://doi.org/10.1016/j.msec.2016.02.078>
- Nair LS, Laurencin CT (2007) Biodegradable polymers as biomaterials. *Prog Polym Sci* 32:762. <https://doi.org/10.1016/j.progpolymsci.2007.05.017>
- Rasal RM, Janorkar AV, Hirt DE (2010) Poly(lactic acid) modifications. *Prog Polym Sci* 35:338. <https://doi.org/10.1016/j.progpolymsci.2009.12.003>
- Jamshidian M, Tehrani EA, Imran M, Jacquot M, Desobry S (2010) Poly-lactic acid: production, applications, nanocomposites, and release studies. *Compreh Rev Food Sci Food Safety* 9:552. <https://doi.org/10.1111/j.1541-4337.2010.00126.x>
- Lasprilla AJR, Martinez GAR, Lunelli BH, Jardini AL, Filho RM (2012) Poly-lactic acid synthesis for application in biomedical devices—A review. *Biotechnol Adv* 30:321. <https://doi.org/10.1016/j.biotechadv.2011.06.019>
- Castro-Aguirre E, Iñiguez-Franco F, Samsudin H, Fang X, Auras R (2016) Poly(lactic acid)—mass production, processing, industrial applications, and end of life. *Adv Drug Deliv Rev* 107:333. <https://doi.org/10.1016/j.addr.2016.03.010>
- Tyler B, Gullotti D, Mangraviti A, Utsuki T, Brem H (2016) Poly(lactic acid) (PLA) controlled delivery carriers for biomedical applications. *Adv Drug Deliv Rev* 107:163. <https://doi.org/10.1016/j.addr.2016.06.018>
- Lassalle V, Ferreira ML (2007) PLA nano- and microparticles for drug delivery: an overview of the methods of preparation. *Macromol Biosci* 7:767. <https://doi.org/10.1002/mabi.200700022>
- Rancan F, Papakostas D, Hadam S et al (2009) Investigation of polylactic acid (pla) nanoparticles as drug delivery systems for local dermatotherapy. *Pharm Res* 26:2027. <https://doi.org/10.1007/s11095-009-9919-x>
- North SH, Lock EH, Cooper CJ, Franek JB, Taitt CR, Walton SG (2010) Plasma-based surface modification of polystyrene microtiter plates for covalent immobilization of biomolecules. *ACS Appl Mater Interfaces* 2:2884. <https://doi.org/10.1021/am100566e>
- Stratton S, Shelke NB, Hoshino K, Rudraiah S, Kumbar SG (2016) Bioactive polymeric scaffolds for tissue engineering. *Bioact Mater* 1:93. <https://doi.org/10.1016/j.bioactmat.2016.11.001>
- Venkatesan J, Bhatnagar I, Manivasagan P, Kang K-H, Kim S-K (2015) Alginate composites for bone tissue engineering: a review. *Int J Biol Macromol* 72:269. <https://doi.org/10.1016/j.ijbiomac.2014.07.008>
- Li B, Kan L, Zhang X et al (2017) Biomimetic bone-like hydroxyapatite by mineralization on supramolecular porous fiber networks. *Langmuir* 33:8493. <https://doi.org/10.1021/acs.langmuir.7b02394>

- [21] Ivanova AA, Syromotina DS, Shkarina SN et al (2018) Effect of low-temperature plasma treatment of electrospun polycaprolactone fibrous scaffolds on calcium carbonate mineralisation. *RSC Adv* 8:39106. <https://doi.org/10.1039/C8RA07386D>
- [22] Shi X, Jiang J, Sun L, Gan Z (2011) Hydrolysis and biomineralization of porous PLA microspheres and their influence on cell growth. *Colloids Surf, B* 85:73. <https://doi.org/10.1016/j.colsurfb.2010.11.016>
- [23] Li LH (2011) Rapid biomimetic mineralization of chitosan scaffolds with a precursor sacrificed method in ethanol/water mixed solution. *Express Polym Lett* 5:545. <https://doi.org/10.3144/expresspolymlett.2011.53>
- [24] Chen J, Chu B, Hsiao BS (2006) Mineralization of hydroxyapatite in electrospun nanofibrous poly(L-lactic acid) scaffolds. *J Biomed Mater Res, Part A* 79A:307. <https://doi.org/10.1002/jbm.a.30799>
- [25] Knill CJ, Kennedy JF (2003) Degradation of cellulose under alkaline conditions. *Carbohydr Polym* 51:281. [https://doi.org/10.1016/S0144-8617\(02\)00183-2](https://doi.org/10.1016/S0144-8617(02)00183-2)
- [26] Lam CX, Teoh SH, Hutmacher DW (2007) Comparison of the degradation of polycaprolactone and polycaprolactone- β -tricalcium phosphate scaffolds in alkaline medium. *Polym Int* 56:718. <https://doi.org/10.1002/pi.2195>
- [27] Zhao Y, Zhang Y, Ning F, Guo D, Xu Z (2007) Synthesis and cellular biocompatibility of two kinds of HAP with different nanocrystal morphology. *J Biomed Mater Res B Appl Biomater* 83B:121. <https://doi.org/10.1002/jbm.b.30774>
- [28] Tsougeni K, Vourdas N, Tserepi A, Gogolides E, Cardinaud C (2009) Mechanisms of oxygen plasma nanotexturing of organic polymer surfaces: from stable super hydrophilic to super hydrophobic surfaces. *Langmuir* 25:11748. <https://doi.org/10.1021/la901072z>
- [29] Parvinzadeh Gashti M, Hegemann D, Stir M, Hulliger J (2014) Thin film plasma functionalization of polyethylene terephthalate to induce bone-like hydroxyapatite nanocrystals. *Plasma Processes Polym* 11:37. <https://doi.org/10.1002/ppap.201300100>
- [30] Murphy WL, Kohn DH, Mooney DJ (2000) Growth of continuous bonelike mineral within porous poly(lactide-co-glycolide) scaffolds in vitro. *J Biomed Mater Res* 50:50. [https://doi.org/10.1002/\(sici\)1097-4636\(200004\)50:1%3c50:Aid-jbm8%3e3.0.Co;2-f](https://doi.org/10.1002/(sici)1097-4636(200004)50:1%3c50:Aid-jbm8%3e3.0.Co;2-f)
- [31] Xu G, Aksay IA, Groves JT (2001) Continuous crystalline carbonate apatite thin films a biomimetic approach. *J Am Chem Soc*. <https://doi.org/10.1021/ja002537i>
- [32] Oyane A, Uchida M, Yokoyama Y, Choong C, Triffitt J, Ito A (2005) Simple surface modification of poly(ϵ -caprolactone) to induce its apatite-forming ability. *J Biomed Mater Res, Part A* 75A:138. <https://doi.org/10.1002/jbm.a.30397>
- [33] N-u-H Saddiqi D, Patra SS (2017) Hydroxyapatite biomineralization on functionalized silicone nanofilaments. *Coll Interf Sci Communi* 16:1. <https://doi.org/10.1016/j.colcom.2016.12.002>
- [34] Xie R, Feng Z, Li S, Xu B (2011) EDTA-assisted self-assembly of fluoride-substituted hydroxyapatite coating on enamel substrate. *Cryst Growth Des* 11:5206. <https://doi.org/10.1021/cg101708y>
- [35] Fujishiro Y, Sato T, Okuwaki A (1995) Coating of hydroxyapatite on metal plates using thermal dissociation of calcium-EDTA chelate in phosphate solutions under hydrothermal conditions. *J Mater Sci - Mater Med* 6:172. <https://doi.org/10.1007/bf00120295>
- [36] Fujishiro Y, Fujimoto A, Sato T, Okuwaki A (1995) Coating of hydroxyapatite on titanium plates using thermal dissociation of calcium-edta chelate complex in phosphate solutions under hydrothermal conditions. *J Colloid Interface Sci* 173:119. <https://doi.org/10.1006/jcis.1995.1304>
- [37] Yabutsuka T, Fukushima K, Hiruta T, Takai S, Yao T (2017) Effect of pores formation process and oxygen plasma treatment to hydroxyapatite formation on bioactive PEEK prepared by incorporation of precursor of apatite. *Mater Sci Eng, C* 81:349. <https://doi.org/10.1016/j.msec.2017.07.017>
- [38] Song M-J, Amirian J, Linh NTB, Lee B-T (2017) Bone morphogenetic protein-2 immobilization on porous PCL-BCP-Col composite scaffolds for bone tissue engineering. *J Appl Polym Sci* 134:45186. <https://doi.org/10.1002/app.45186>
- [39] Kepa K, Coleman R, Grøndahl L (2015) In vitro mineralization of functional polymers. *Biosurf Biotribol* 1:214. <https://doi.org/10.1016/j.bsbt.2015.09.001>
- [40] Schneider M, Günter C, Taubert A (2018) Co-deposition of a hydrogel/calcium phosphate hybrid layer on 3d printed poly(lactic acid) scaffolds via dip coating: towards automated biomaterials fabrication. *Polymers* 10:275
- [41] Liguori A, Bigi A, Colombo V et al (2016) Atmospheric pressure non-equilibrium plasma as a green tool to crosslink gelatin nanofibers. *Sci Rep* 6:38542. <https://doi.org/10.1038/srep38542>
- [42] Ntalianas HA, Whitney RM (1964) Calcein as an indicator for the determination of total calcium and magnesium and calcium alone in the same aliquot of milk. *J Dairy Sci* 47:19. [https://doi.org/10.3168/jds.S0022-0302\(64\)88575-1](https://doi.org/10.3168/jds.S0022-0302(64)88575-1)
- [43] Thomas V, Kumari TV, Jayabalan M (2001) In vitro studies on the effect of physical cross-linking on the biological performance of aliphatic poly (urethane urea) for blood contact applications. *Biomacromolecules* 2(2):588–596
- [44] Tucker BS, Aliakbarshirazi S, Vijayan VM, Thukkaram M, De Geyter N, Thomas V (2021) Non-thermal plasma processing for nanostructured biomaterials and tissue

engineering scaffolds: a mini review. *Cur Opin Biomed Eng.* <https://doi.org/10.1016/j.cobme.2020.100259>

[45] Baptista R, Guedes M, Pereira MFC, Mauricio A, Carrelo H, Cidade T (2020) On the effect of design and fabrication parameters on mechanical performance of 3D printed PLA

scaffolds. *Bioprinting* 20:e00096. <https://doi.org/10.1016/j.bioprint.2020.e00096>

Publisher's Note Springer Nature remains neutral with regard to jurisdictional claims in published maps and institutional affiliations.